Nami, A., Rodriguez-Amenedo, J. L., Arnaltes, S., Cardiel-Alvarez, M. A. & Baraciarte, R. A. (2020). Frequency Control of Offshore Wind Farm With Diode-Rectifier-based HVdc Connection. *IEEE Transactions on Energy Conversion*, 35(1), pp. 130–138.

DOI: 10.1109/tec.2019.2949892

Frequency Control of Offshore Wind Farm with Diode Rectifier-based HVDC Connection

Ashkan Nami, Jose Luis Rodriguez-Amenedo, *Member, IEEE,* Santiago Arnaltes, Miguel Ángel Cardiel-Álvarez, and Roberto Alves Baraciarte

***Abstract*—This paper presents a direct frequency control for offshore wind farms (OWFs) connected to the diode rectifier (DR)-based high voltage direct current (HVDC) link. The frequency control is guaranteed through reactive power balance at the DR station without a capacitor bank placed at the DR station; while AC-voltage magnitude is clamped by the DR, provided that the HVDC link voltage is imposed by the onshore inverter. The control system is implemented by a voltage source converter (VSC) connected to the DR station. The VSC is also used to compensate harmonic currents, leading to passive AC-filters being also removed from the DR station. The proposed control system provides comparative advantages in terms of DR station volume and OWF installation cost with other centralized controls where besides a VSC, a high-voltage large capacitor bank is needed to be placed at the DR station. A new average-value model (AVM) of the DR system is derived to test the proposed frequency control, while the stability of the system is evaluated through a small-signal analysis. The proposed control system performance and the accuracy of the proposed AVM are verified through a detailed switching model of the system using operation of a cascaded H-bridge VSC.**

***Index Terms*—Offshore wind farm (OWF), high voltage direct current (HVDC), diode rectifier (DR), voltage source converter (VSC), frequency control, average-value model (AVM).**

I. Introduction

NOWADAYS, renewable energy generation is very important due to the target of reducing greenhouse gas emissions in electricity generation. The better offshore wind conditions in terms of wind speed and resource availability have made offshore wind farms (OWFs) to be an emerging electricity generation solution. The distance from an OWF to the onshore defines the interconnection to be used [1]. Therefore, for OWFs situated far away from the onshore, high voltage direct current (HVDC) links are the preferred technology.

Current OWF projects with HVDC connection use voltage source converter (VSC) in the offshore rectifier station. But, the possibility of using diode rectifier (DR) in the offshore substation which was first reported in [2], has recently received an increasing interest given its lower cost and losses together with its higher reliability compared to the VSC-based HVDC [3]. A compact solution with DR integrated in the transformer oil insulation is presented in [2] leading to the volume of the offshore platforms and as a result, the installation and maintenance costs being reduced considerably [4]. However, this solution requires passive AC-filters to be placed at the DR station to improve its performance. Moreover, an umbilical cable interconnecting the onshore to the offshore AC-grid proposed in [2] is needed for the black start of OWFs connected to the DR-based HVDC link. But, the main drawback of the DR solution for OWF applications is that the system frequency has to be controlled to guarantee the DR commutation, given that the isolated offshore AC-grid can not generate the required frequency with the conventional wind turbine (WT) control systems. There are two different frequency control solutions addressed in the literature to overcome this drawback: distributed and centralized.

In distributed solutions, the capability of wind turbine generator systems (WTGSs) is used to impose the system frequency depending on the type of WTs used, thereby changing in all the conventional WT control systems. A distributed frequency control implemented by type-4 WTs is presented in [5], which is derived from the dynamics of a capacitor bank placed at the DR station. However, it depends on many measurements and needs the point of common coupling (PCC) voltage angle to be sent to WTs controller through a communication channel, further failing in robustness. Using the same control strategy, the proposal in [6] allows a distributed frequency control with reduced passive filter banks placed at the DR station, thereby improving the offshore platforms footprint. In [7], type-3 and type-4 WTs behave as AC-voltage sources controlling their terminal voltages using standard P/f and Q/V droops. Therefore, in this solution, the PCC voltage magnitude is controlled to transfer the desired power reference. But, in [8], P/V and Q/f droops are used where communications between WTs are needed. These communications are supposed to be removed in [9]. Nevertheless, the control still needs a remote voltage angle to be received in WTs controller, and it has to be through communications which are not considered. In [10] and [11], a Q/f droop is proposed in which communications between WTs are not needed, while no phase-locked loop (PLL) is used in [11]. The use of global positioning system (GPS) signal is proposed in [12] and [13] to synchronize all WTs current injections. This way the reactive power of each of the WTs is not controlled and, as a result, they could exceed their limits. A droop is proposed to overcome this drawback, but it couples the active and reactive power control of WTs. In [14], a control based on adding parallel and orthogonal components to the terminal voltages of WTs is proposed which relies on centralized and decentralized measurements. A distributed solution for OWFs connected to the thyristor rectifier (TR) is also presented in [15], [16]

A. Nami, J.L. Rodriguez-Amenedo, S. Arnaltes and M.Á. Cardiel-Álvarez are with Electrical Engineering Department of Carlos III University of Madrid, Madrid 28911, Spain (e-mail: anami@ing.uc3m.es; amenedo@ing.uc3m.es; arnalte@ing.uc3m.es; 100079288@alumnos.uc3m.es).

R. Alves Baraciarte is with ABB Corporate Research, Västerås, Sweden (e-mail: roberto.alves@se.abb.com).

and [17] where the terminal voltages of the type-3 WTs are controlled and the active power balance at the TR station is adjusted by modifying the TR firing angle needed for the frequency control. Thus, this control is based on a frequency-dependent load.

But, in centralized solutions, a VSC is always needed to be placed at the DR station to generate and control the system frequency. In addition, the VSC can be used for the compensation of DR harmonic currents, leading to the passive AC-filters being partly or completely removed from the DR station. Therefore, the centralized solutions can be implemented irrespective of the type of WTs used. Moreover, the VSC can be used either as STATCOM with battery energy storage system (BESS) integrated or as hybrid HVDC system in DC-series and -parallel connection with the DR to black start of OWFs in such applications. Therefore, the centralized solutions can overcome all the drawbacks of the DR-based HVDC system in which it is not required to change the conventional WT control systems. In [18], [19], [20], [21] and [22], a centralized frequency control using STATCOM for OWFs connected to the TR is proposed. The STATCOM placed at the TR station behaves as a slack bus and the TR firing angle is needed to adjust the active power unbalancing detected by the variations on the STATCOM DC-link. Therefore, this approach becomes unfeasible with the DR solution. Concerning the DR solution, a centralized frequency control using a hybrid HVDC system consisting of the DC-series connection of a 12-pulse DR and a two-level VSC is proposed in [23]. In this proposal, the VSC controls the AC-voltage magnitude together with its DC-link voltage using a voltage oriented control, leading to one third of OWF rated power being transmitted through the VSC. The same DC-series hybrid topology is used in [24] and [25], while the two-level VSC is replaced by a modular multilevel converter (MMC) in [25] used for the black start of OWFs and the DC-ripple compensation during the DR operation. However, in both approaches, WTs are responsible for the frequency control. Furthermore, as another functionality of the VSC, an active power filter (APF) scheme is implemented in [23] and [24] to reach reduced DR passive AC-filters. In [26], the parallel operation of DR and VSC is reported as a centralized solution where its economic benefits compared to the VSC-based HVDC are studied. Moreover, a hybrid HVDC system consisting of DC-parallel connection of a 12-pulse DR and a VSC is proposed in [27] where an additional DC/DC power conversion is required to reduce the rated DC-voltage of the VSC. The VSC power demand for OWF black start, frequency control and harmonic current compensation is studied as well. However, in these proposals, passive AC-filter banks are still needed to be placed at the DR station to remove low-order harmonics from the AC-voltage.

In [28], the principles of a direct frequency control using reactive power balance at the DR station bus are proposed. This can be achieved through a controlled reactive power generated by a VSC placed at the DR station. The VSC power demand for the frequency control depends on the system and control parameters and the transients in the system, as analyzed in [29]. However, this centralized solution is derived from an average-value model (AVM) of the DR system where

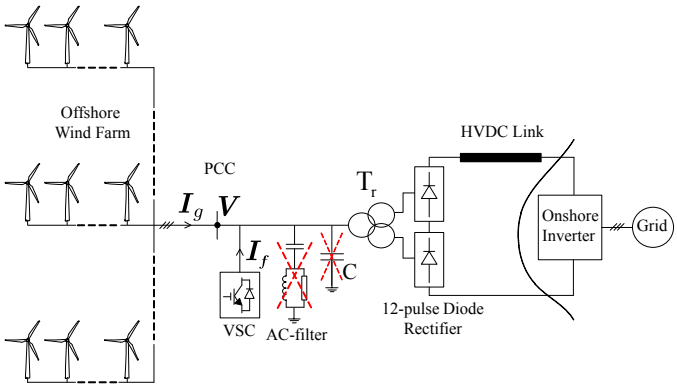

Fig. 1. Proposed system: Using a VSC for connection of an OWF through the DR-based HVDC link without a capacitor bank placed at the DR station.

a high voltage large capacitor bank is also needed to be placed at the DR station. This demands larger offshore platforms for the DR stations, further increasing the OWF installation cost. Using the same control strategy, [29] presents an APF scheme embedded in the frequency control, which is implemented by a VSC placed at the DR station, thereby removing the DR passive AC-filters. However, a capacitor bank is still needed to be placed at the DR station for the frequency control.

This paper presents a direct frequency control which allows the connection of an OWF through the DR-based HVDC system without a capacitor bank placed at the DR station. The proposed control system is implemented by a VSC connected to the DR station bus; while the AC-voltage magnitude is clamped by the DR, provided that the HVDC link voltage is imposed by the onshore inverter. In addition, the VSC is used for the DR harmonic currents compensation, resulting in no passive AC-filters being required at the DR station as well. Therefore, using the proposed control system, the required DR station volume and as a result, the OWF installation cost can be relatively reduced in comparison with other centralized solutions in which besides a VSC, a high voltage large capacitor bank is also needed to be placed at the DR station. A new AVM of the DR system for such applications is also derived to test the proposed frequency control principles, while the stability of the system with embedded frequency control is proved by a small signal analysis. Furthermore, the performance of the proposed control system as well as the accuracy of the proposed AVM are verified through the detailed switching model (DSM) of the system using the operation and control of a delta-connected cascaded H-bridge (CHB) VSC, which is the most attractive topology for high voltage applications.

II. System Description

Fig. 1 shows an OWF connected to the onshore grid through the DR-based HVDC link. The DR station consists of a twelve-pulse diode bridge connected to the PCC through a transformer T_r. A VSC is connected to the DR station bus, that is always needed for the centralized frequency control of the isolated offshore AC-grid in opposition to the decentralized control [11]. But, the high voltage large capacitor bank C, which was originally needed for the objective of derivation of the

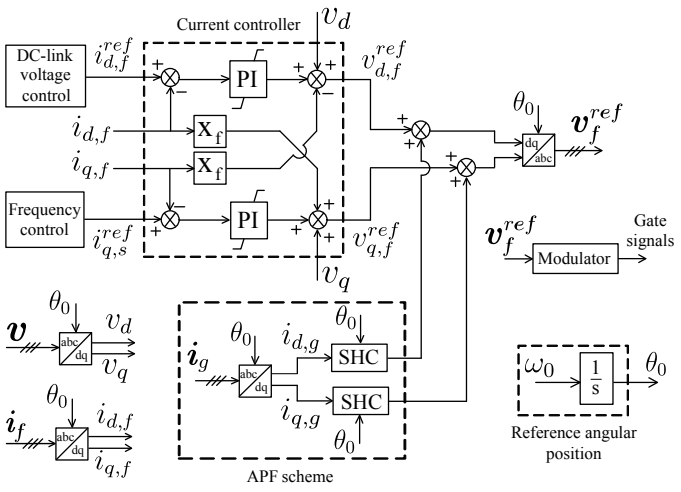

Fig. 2. Overall control scheme of the VSC.

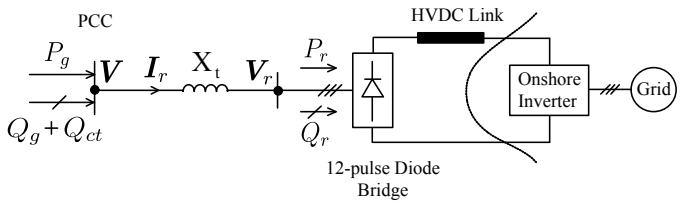

Fig. 3. Simplified model of the system.

frequency control principles, is removed from the DR station, given the proposed control system (described in Subsection III-B). In addition, the VSC is used to compensate harmonic currents generated by the DR, thereby removing passive AC-filters from the DR station as well. The VSC current injected to the DR station bus is $\boldsymbol{I_f}$, while $\boldsymbol{I_g}$ is the offshore AC-grid current flowing into the PCC, the PCC voltage being $\boldsymbol{V}$. Note that the onshore inverter can be line-commutated converter (LCC) or VSC, but it has to be operated in constant DC-voltage mode for successful operation of the system.

III. Control Strategy

In this section, the required VSC control scheme implemented in the synchronous (dq) reference frame is presented. Note that d and q subscripts refer to the corresponding vector components. It is also worth mentioning that, lowercase notation represents the per-unit values of the variables and parameters.

A. Overall Control Scheme

Fig. 2 shows the overall control scheme in which the required VSC reference voltage ($\boldsymbol{v_f^{ref}}$) for both the frequency control and the harmonic compensation is generated. As observed, d- and q-components of the VSC reference current ($i_{d,f}^{ref}$ and $i_{q,f}^{ref}$) are given by the DC-link voltage control and the proposed frequency control (described in Subsection III-B), respectively. Using the conventional proportional-integral (PI)-based current controller, d- and q-components of the VSC current ($i_{d,f}$ and $i_{q,f}$) are controlled to follow their reference values. This leads to the corresponding vector components of the VSC reference voltage ($v_{d,f}^{ref}$ and $v_{q,f}^{ref}$) being determined. Note that $\mathrm{x_f}$ used in the cross-coupling terms of the controller is the reactance of the VSC line reactor. However, the reference voltages $v_{d,f}^{ref}$ and $v_{q,f}^{ref}$ are needed only for the frequency control and successful operation of the VSC.

Therefore, an APF scheme embedded in the frequency control is also needed for the harmonic current compensation, as shown in Fig. 2. For this purpose, a PI-based selective harmonic compensation (SHC) technique [29] is used in the APF scheme. The SHC is separately carried out on both d- and q-components of the offshore AC-grid current ($i_{d,g}$ and $i_{q,g}$) to eliminate their harmonic orders $h = 12\,k$ ($k = 1, 2, ...$), thereby removing the corresponding harmonic orders from the PCC phase voltages (shown in Subsection VI-B). This leads to d- and q-components of the APF reference voltage being obtained which are added to $v_{d,f}^{ref}$ and $v_{q,f}^{ref}$, respectively. Then, their outputs are transformed back to three-phase quantities to generate $\boldsymbol{v_f^{ref}}$. Finally, by passing $\boldsymbol{v_f^{ref}}$ through the modulator, the required gate signals of the VSC are provided.

Note that the DC-link voltage control scheme and the type of modulation depend on the VSC topology used, whereas the frequency control scheme can be used with any VSC topology. Moreover, the conventional voltage oriented control using PLL, that is needed for the synchronization of the VSC output voltage with the controller reference frame, becomes unfeasible due to the missing AC-voltage source [12]. Therefore, the reference voltage angular position (θ_0) used in the overall control scheme is obtained internally by integrating a desired angular frequency (ω_0), as shown in Fig. 2. As a result, given that no PLL is used, θ_0 is not subject to any grid disturbance.

In the following subsection, the obtainment of the reference $i_{q,f}^{ref}$ needed for the frequency control is described, which is within the scope of this work.

B. Frequency Control

For objective of the derivation of the frequency control principles, Fig. 3 shows a simplified model of the proposed system depicted in Fig. 1. The OWF is represented by the offshore AC-grid active and reactive powers injected to the PCC (P_g and Q_g), which are independent of the WT technology (type-3, type-4, etc.). In addition, a controlled reactive power (Q_{ct}) given by the VSC is injected in the DR station bus. The rectifier transformer is represented by its short-circuit reactance ($\mathrm{X_t}$) whose current is $\boldsymbol{I_r}$. This provides the rectifier AC-side voltage ($\boldsymbol{V_r}$) determining active and reactive powers drawn by the DR (P_r and Q_r).

The dynamics of the simplified model in Fig. 3 represented in the dq reference frame rotating at ω_0 can be written as follows:

$$\underline{\boldsymbol{v}} - \underline{\boldsymbol{v_r}} = \frac{\mathrm{x_t}}{\omega_0}\frac{d\underline{\boldsymbol{i_r}}}{dt} + \mathrm{j}\,\mathrm{x_t}\,\underline{\boldsymbol{i_r}} \tag{1}$$

where $\underline{\boldsymbol{i_r}}$ is the rectifier current vector, and $\underline{\boldsymbol{v}}$ and $\underline{\boldsymbol{v_r}}$ are the PCC and rectifier voltage vectors, respectively. Note that since no PLL is used, the synchronous axis is not oriented on $\underline{\boldsymbol{v}}$ ($v_q \neq 0$), as shown in Fig. 4.

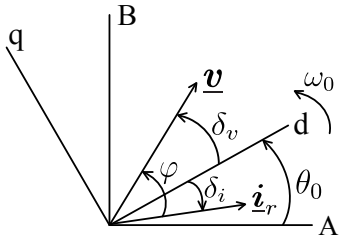

Fig. 4. Vector diagram in both the stationary and synchronous reference frames.

Multiplying both left and right-hand sides of (1) by the conjugate of $\underline{\boldsymbol{i_r}}$, (2) is given.

$$\underline{\boldsymbol{v}}\,\underline{\boldsymbol{i}}_{\boldsymbol{r}}{}^{*} - \underline{\boldsymbol{v}}_{\boldsymbol{r}}\,\underline{\boldsymbol{i}}_{\boldsymbol{r}}{}^{*} = \frac{\mathrm{x_t}}{\omega_0}\,\frac{d\underline{\boldsymbol{i}}_{\boldsymbol{r}}}{dt}\,\underline{\boldsymbol{i}}_{\boldsymbol{r}}{}^{*} + \mathrm{j}\,\mathrm{x_t}\,{i_r}^2 \tag{2}$$

where i_r is the magnitude of $\underline{\boldsymbol{i_r}}$ and * denotes the complex conjugate operator.

Then, the term $\frac{d\underline{\boldsymbol{i}}_{\boldsymbol{r}}}{dt}\,\underline{\boldsymbol{i}}_{\boldsymbol{r}}{}^{*}$ in (2) can be analytically expressed in its dq components as

$$\frac{d\underline{\boldsymbol{i}}_{\boldsymbol{r}}}{dt}\,\underline{\boldsymbol{i}}_{\boldsymbol{r}}{}^{*} = \frac{di_{d,r}}{dt}\,(i_{d,r} - \mathrm{j}\,i_{q,r}) + \frac{di_{q,r}}{dt}\,(i_{q,r} + \mathrm{j}\,i_{d,r}) \tag{3}$$

Using this expression, (2) can be split in its real and imaginary terms in the following set of equations:

$$p_g - p_r = \frac{\mathrm{x_t}}{\omega_0}\,(i_{d,r}\,\frac{di_{d,r}}{dt} + i_{q,r}\,\frac{di_{q,r}}{dt}) \tag{4}$$

$$q_g + q_{ct} - q_r - q_t = \frac{\mathrm{x_t}}{\omega_0}\,(-i_{q,r}\,\frac{di_{d,r}}{dt} + i_{d,r}\,\frac{di_{q,r}}{dt}) \tag{5}$$

where $q_t = \mathrm{x_t}\,{i_r}^2$ is the reactive power of the rectifier transformer.

The right-hand sides of (4) and (5) are modified using the transformation from Cartesian to polar coordinates system. This leads to the dynamic equations whose state variables are magnitude and angle of $\underline{\boldsymbol{i_r}}$. For this purpose, a set of equations defining the polar derivatives as a function of the Cartesian derivatives is presented in (6).

$$\begin{aligned} i_r\,\frac{di_r}{dt} &= i_{d,r}\,\frac{di_{d,r}}{dt} + i_{q,r}\,\frac{di_{q,r}}{dt} \\ {i_r}^2\,\frac{d\delta_i}{dt} &= -i_{q,r}\,\frac{di_{d,r}}{dt} + i_{d,r}\,\frac{di_{q,r}}{dt} \end{aligned} \tag{6}$$

where $\delta_i = \delta_v - \varphi$ stands for the angle of $\underline{\boldsymbol{i_r}}$, while δ_v stands for the angle of $\underline{\boldsymbol{v}}$ and φ is the angle between $\underline{\boldsymbol{v}}$ and $\underline{\boldsymbol{i_r}}$, as shown in Fig. 4.

Using the expressions in (6), the dynamic equations (4) and (5) can be rewritten as follows:

$$\frac{1}{\omega_0}\,\frac{di_r}{dt} = \frac{i_r}{q_t}\,(p_g - p_r) \tag{7}$$

$$\frac{1}{\omega_0}\,\frac{d\delta_i}{dt} = \frac{q_g + q_{ct} - q_r}{q_t} - 1 \tag{8}$$

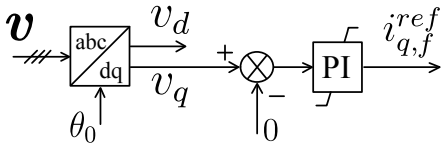

Fig. 5. Proposed frequency control scheme.

According to (8), the reactive power balance at the PCC determines the dynamic of δ_i, further driving the dynamic response of δ_v. Then, the frequency control can be guaranteed by maintaining δ_v equal to zero in order to align $\underline{\boldsymbol{v}}$ along the d-axis (v_q = 0) as the synchronous axis rotates at the desired frequency (e.g. 50 Hz). This is used to derive the frequency control principles based on the control of the q-component of the PCC voltage v_q in the dq reference frame which is generated internally. Furthermore, given that the system frequency can be expressed as $\omega = \omega_0 + \frac{d\delta_v}{dt}$, (8) can be transformed into a certain expression of frequency depending on the reactive power balance at the PCC as follows:

$$\frac{\omega}{\omega_0}\,q_t = q_g + q_{ct} - q_r \tag{9}$$

However, in the reactive power balance stated in (9), both q_r and q_t are the reactive powers drawn by the DR station depending on the active power transmitted which can not be controlled. Moreover, the incoming OWF reactive power q_g depends on the power factor settings at the WTGSs and the length of the AC-cables. Therefore, the additional q_{ct} generated by the VSC can be used to achieve the reactive power balance and as a result, to guarantee the frequency control. Note that the maximum instantaneous q_{ct} depends of the system and control parameters and the transients in the system [29]. Finally, according to the aforementioned explanations, the proposed frequency control scheme is derived where v_q is controlled to be zero (δ_v = 0) using a PI controller resulting in the q-component of the VSC reference current $i_{q,f}^{ref}$ being set, as shown in Fig. 5.

Furthermore, according to (7), the active power balance in the DR station bus determines the dynamic of i_r. Given that i_r is proportional to the DR DC-current in the per-unit system [28], the dynamic of the DR DC-voltage is also determined by the active power balance based on the HVDC link model. As a result, due to the relationship between AC and DC-voltages of the DR [30] and [31], the active power balance in the DR station bus drives the dynamic response of the PCC voltage magnitude. Therefore, as can be seen in Fig. 5, the d-component of the PCC voltage v_d defining the PCC voltage magnitude remains uncontrolled and it automatically accommodates the voltage required for transmitting the power through the DR (shown in Section VI). This way the system frequency is controlled by regulation of v_q while the PCC voltage magnitude v_d is clamped by the DR operation, provided that the HVDC link voltage is imposed by the onshore inverter. This makes the difference between the proposed control system and the conventional VSC-based grid forming using inner current control in which VSC behaves as a slack bus through regulation of the AC-

voltage magnitude [32]. Moreover, the operation and control of the VSC used in the proposed system are different from the conventional STATCOM in which reactive power is generated through regulation of the AC-voltage magnitude.

IV. Diode Rectifier Station Modelling

In this section, the AVM of the DR station and the HVDC link is derived which is used to test the proposed frequency control principles. For this purpose, the HVDC link is represented by a lumped T-model given in [33]. In addition, given the onshore inverter operation in constant DC-voltage mode, the inverter station is modelled as a DC-voltage source.

According to the aforementioned assumptions, Fig. 6a shows the considered DR-based HVDC system to be modelled with its corresponding input and output signals. As observed, the DC-cable is represented by its parallel capacitor $\mathrm{c_c}$ whose voltage is v_c and two series resistor-inductor branches depicted by $\mathrm{r_{dc1}}$, $\mathrm{l_{dc1}}$ and $\mathrm{r_{dc2}}$, $\mathrm{l_{dc2}}$. This provides two different DC-currents: The rectifier DC-current i_{dc1} and the inverter DC-current i_{dc2}, respectively. Moreover, the DC-voltage input at the inverter station is v_{di}, while the rectifier DC-voltage is v_{dr}. Finally, v is the magnitude of the PCC voltage vector. Note that, in this study case, the rectifier losses and system harmonics are neglected, and the rectifier station consists of a twelve-pulse diode bridge.

Considering the model in Fig. 6a, the dynamic equations regarding the DC-side of the system are given in (10)-(12).

$$v_{dr} - v_c = \mathrm{r_{dc1}}\, i_{dc1} + \frac{\mathrm{l_{dc1}}}{\omega_0}\,\frac{di_{dc1}}{dt} \tag{10}$$

$$i_{dc1} - i_{dc2} = \frac{\mathrm{c_c}}{\omega_0}\,\frac{dv_c}{dt} \tag{11}$$

$$v_c - v_{di} = \mathrm{r_{dc2}}\, i_{dc2} + \frac{\mathrm{l_{dc2}}}{\omega_0}\,\frac{di_{dc2}}{dt} \tag{12}$$

Then, using the expression in (10), the rectifier power balance is assumed given by:

$$p_r = p_{dr} = \mathrm{r_{dc1}}\, {i_{dc1}}^2 + \frac{\mathrm{l_{dc1}}}{\omega_0}\, i_{dc1}\,\frac{di_{dc1}}{dt} + v_c\, i_{dc1} \tag{13}$$

where $p_{dr} = i_{dc1}\, v_{dr}$ is the rectifier DC-power.

In a per-unit system, the rectifier AC-current magnitude i_r is equal to $k_\mu\, i_{dc1}$ ($i_r = k_\mu\, i_{dc1}$) [28] where k_μ depends on the commutation angle μ as detailed in Appendix A. By substituting the aforementioned expressions of p_r and i_r in (7), the final dynamic equations of the proposed model (14)-(17) are derived.

$$f_1 = \frac{1}{\omega_0}\,\frac{d\delta_i}{dt} = \frac{q_g + q_{ct} - q_r}{q_t} - 1 \tag{14}$$

$$f_2 = \frac{1}{\omega_0}\,\frac{di_{dc1}}{dt} = \frac{i_{dc1}\,(p_g - \mathrm{r_{dc1}}\, {i_{dc1}}^2 - v_c\, i_{dc1})}{q_t + \mathrm{l_{dc1}}\, {i_{dc1}}^2} \tag{15}$$

$$f_3 = \frac{1}{\omega_0}\,\frac{dv_c}{dt} = \frac{i_{dc1} - i_{dc2}}{\mathrm{c_c}} \tag{16}$$

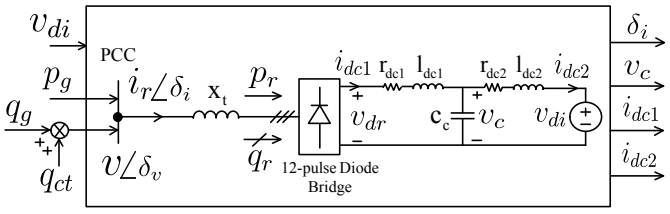

(a) DR system to be modelled: Input and output signals of the proposed AVM

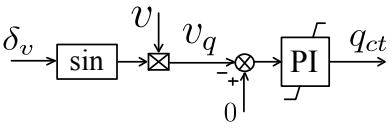

(b) Frequency control scheme for the proposed AVM

Fig. 6. Overall scheme of the proposed AVM.

$$f_4 = \frac{1}{\omega_0}\,\frac{di_{dc2}}{dt} = \frac{v_c - v_{di} - \mathrm{r_{dc2}}\, i_{dc2}}{\mathrm{l_{dc2}}} \tag{17}$$

However, besides these dynamic equations, some algebraic expressions are needed for the model to determine the undefined variables. For this purpose, by substituting (15) in (10), the algebraic expression defining the value of v_{dr} is given by:

$$v_{dr} = \mathrm{r_{dc1}}\, i_{dc1} + \frac{\mathrm{l_{dc1}}\, i_{dc1}\,(p_g - \mathrm{r_{dc1}}\, {i_{dc1}}^2 - v_c\, i_{dc1})}{q_t + \mathrm{l_{dc1}}\, {i_{dc1}}^2} + v_c \tag{18}$$

This expression, along with the algebraic equation (A.3) detailed in Appendix A, yield the values of v and φ. Then, the value of δ_v can be defined as $\delta_v = \delta_i + \varphi$ (Fig. 4). In addition, the total reactive power value of the rectifier plus its transformer ($q_r + q_t$) is determined as follows:

$$q_r + q_t = p_g \tan\varphi \tag{19}$$

where $q_t = \mathrm{x_t}\,(k_\mu\, i_{dc1})^2$, resulting in the value of q_r being defined.

Finally, the dynamic equations (14)-(17), along with the above-mentioned algebraic expressions and extra algebraic equations detailed in Appendix A, constitute the proposed AVM of the DR system depicted in Fig. 6a. Therefore, the required input signals for the proposed model are the inverter DC-voltage (v_{di}), the incoming offshore AC-grid active and reactive powers (p_g and q_g) and the controlled reactive power (q_{ct}); while the outputs are the system states, as can be seen in Fig. 6a. Note that the proposed model is a totally new AVM of the DR system as it does not require the dynamics of a capacitor placed at the DR station to produce the outputs [28]. Moreover, Fig. 6b shows the frequency control scheme for the proposed AVM to determine the value of q_{ct} based on the previously proposed frequency control principles. As observed, the q-component of the PCC voltage v_q is defined as $v_q = v \sin\delta_v$ using the output signals of the model. Then, v_q is regulated to be zero through a PI controller, resulting in the value of q_{ct} being set.

V. Control System Stability Analysis

In this section, the stability of the system with embedded frequency control is evaluated using the small-signal studies. For this purpose, the expression for the corresponding PI frequency controller in the small-signal is presented in (20). Note that subscript 0 refers to the steady-state value of the variables.

$$\Delta q_{ct} = -(k_p\,\Delta v_q + k_i\,\omega_0 \int \Delta v_q\,dt) \tag{20}$$

where $\Delta v_q = v_0\,\Delta\delta_v = v_0\,(\Delta\delta_i + \Delta\varphi)$, provided that δ_v equals zero in steady-state. k_p and k_i are the proportional and integral control parameters of the PI controller, respectively.

Substituting the expression of Δv_q in (20) defines a new state Δx_5, further adding a new dynamic equation to the system given in (21).

$$f_5 = \frac{1}{\omega_0}\frac{d\Delta x_5}{dt} = \Delta\delta_i + \Delta\varphi \tag{21}$$

In addition, the system's dynamic model given in (14)-(17) is linearized around a steady-state operating point to analyze the stability of the control system through its eigenvalues. Then, the corresponding small-signal equations are as follows:

$$\frac{1}{\omega_0}\frac{d\Delta x}{dt} = A\,\Delta x + B\,\Delta u$$

$$\Delta y = C\,\Delta x + D\,\Delta u \tag{22}$$

where $\Delta x = [\Delta\delta_i, \Delta i_{dc1}, \Delta v_c, \Delta i_{dc2}, \Delta x_5]^\top$,
$\Delta y = [\Delta\delta_v, \Delta v, \Delta i_{dc1}, \Delta v_c, \Delta i_{dc2}, \Delta q_{ct}]^\top$ and
$\Delta u = [\Delta p_g, \Delta q_g, \Delta v_{di}]^\top$.

However, in order to derive the linearized system, the algebraic equations detailed in Section IV and Appendix A are needed for the obtainment of the matrices A-D. Note that, in this study, variable k_μ used in the proposed model is assumed constant with a value equal to steady-state [28].

Fig. 7a shows the eigenvalues of the system at different active power operating points. The eigenvalues are obtained under a hundred incoming active power operating points between p_{g0} = 0.01 p.u. and p_{g0} = 1 p.u. with the required input parameters detailed in Appendix B. Note that, for the sake of clarity, the least relevant eigenvalues which are the ones with the non-positive real part far away from the imaginary axis are not shown here. Furthermore, the arrows in Fig. 7a indicate the movement of the system eigenvalues based on the active power increment and dominant state variables are shown for each of the eigenvalues. As observed, the real part of the obtained eigenvalues is negative which proves the control system stability in all operating points. The zoomed view of the complex eigenvalues whose dominant state is Δv_c is depicted in Fig. 7b. These eigenvalues are damped by increasing the incoming active power, with the movement of the eigenvalues towards more stable points. In addition, Δx_5 in Fig. 7b is the dominant state variable of the eigenvalues which does not depend on the operating points.

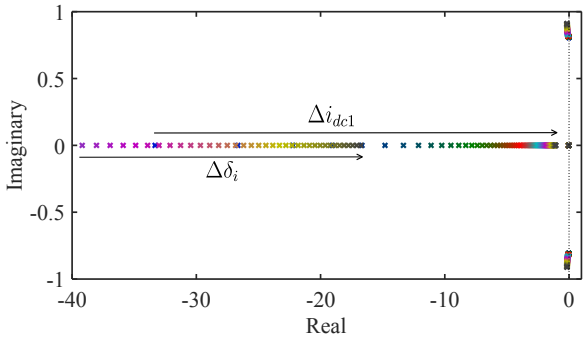

(a) Overall view

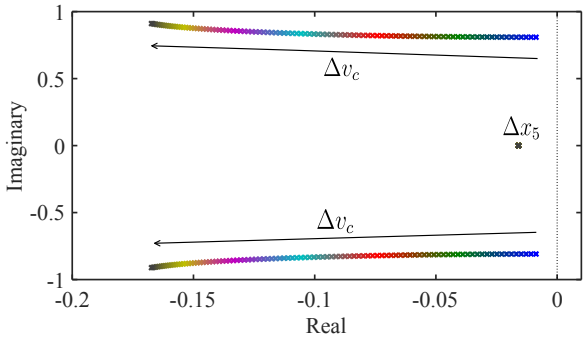

(b) Zoomed view around the imaginary axis

Fig. 7. Small-signal studies: Eigenvalues of the control system at different active power operating points (arrows indicate increasing active power).

VI. Simulation Results

In this section, the performance of the proposed control system has been tested through two different simulations: The AVM simulation and the DSM simulation. In the first, the proposed model with embedded frequency control derived in Section IV (Fig. 6) has been simulated for different study cases in MATLAB/Simulink using the system and control parameters detailed in Appendix B. In the second, one of those study cases has been implemented in the DSM of the proposed system (described in Subsection VI-B), while the accuracy of the proposed AVM has been verified.

A. Average-value Model Simulation Results

Two different initial OWF incoming active powers p_{g01} = 0.1 p.u. and p_{g02} = 0.8 p.u. have been considered for the simulation of the proposed AVM. Furthermore, the initial incoming reactive power for both cases is zero. Then, the performance of the proposed model has been tested by applying two scheduled input changes. In the first, the incoming active power p_g has increased by 0.2 p.u. at t = 0.01 s. In the second, the incoming reactive power q_g has increased by 0.1 p.u. at t = 0.3 s.

Finally, Fig. 8 shows the simulation results of the proposed AVM for both cases where the dynamic response of controlled reactive power q_{ct}, frequency f and PCC voltage magnitude v are presented. It is worth mentioning that the reactive power drawn by the DR station increases with the increment of the active power transmitted. Therefore, as observed, the initial value of q_{ct} set by the frequency control scheme depicted in Fig. 6b has increased for the higher p_{g0} to satisfy the reactive power balance at the PCC needed for the frequency

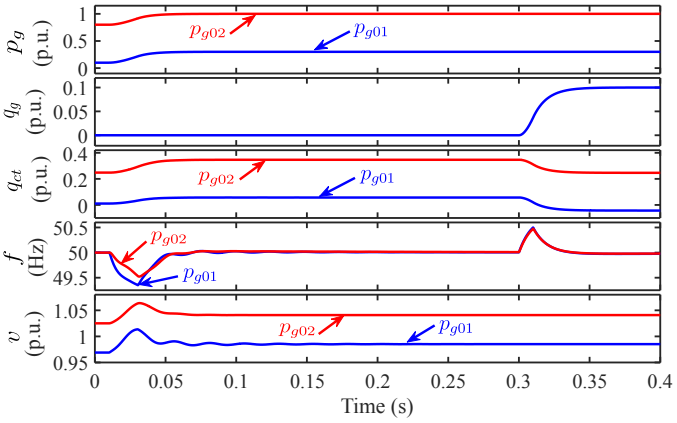

Fig. 8. Controlled reactive power, frequency and PCC voltage magnitude during incoming active and reactive power changes for the AVM.

control. The initial value of v has also increased for p_{g02} as a consequence of higher initial active power which is clamped by the DR, provided that the HVDC link is imposed by the onshore inverter.

According to the aforementioned explanations, both q_{ct} and v increase with the active power increment at t = 0.01 s. However, v has not been affected by the change of q_g at t = 0.3 s while q_{ct} decreases to maintain the frequency at its reference value (50 Hz). Note that the system's dynamic response to the active power increment in the case with p_{g01} oscillates more compared to the one with p_{g02}. This result can be proved by the small-signal studies carried out in Section V where the complex eigenvalues are damped with the active power increment, as shown in Fig. 7b. Moreover, the steady-sate response of v during the scheduled active power changes proves that the DR acts as a voltage clamp on v in this system.

B. Detailed Switching Model Simulation Results

Fig. 9a shows the considered OWF for the DSM simulation of the proposed control system, which has been fully built in MATLAB/Simulink with the system and control parameters detailed in Appendix B. The DR station consists of the nonlinear model of a 12-pulse DR given by the Simulink Library Browser (Simscape/Power Systems). A CHB VSC has been considered in this study case for both the frequency control and the harmonic compensation through generating a controlled reactive power (Q_{ct}). For this purpose, a full DSM of the CHB VSC has also been built in MATLAB/Simulink consisting of three identical clusters with a delta connection, as shown in Fig. 9b. Each cluster consists of a number of series-connected H-bridges to reach the AC-voltage level depending on the H-bridges DC-link rated voltages and is connected as the delta branch through the reactance $\mathrm{X_f}$. The IGBTs used in the H-bridges have also been given by the Simscape/Power Systems and their corresponding gate signals have been provided through the overall control scheme previously described in Subsection III-A (Fig. 2), leading to the modulated cluster voltages $V_{ab,f}$, $V_{bc,f}$ and $V_{ca,f}$ being generated. Note that the model predictive control (MPC) technique [34] has been used in the modulator block to obtain the CHB VSC switching

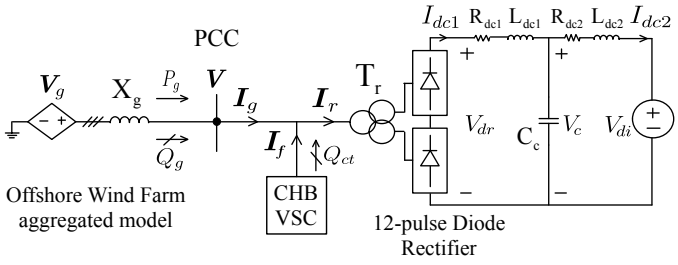

(a) Considered OWF to be simulated

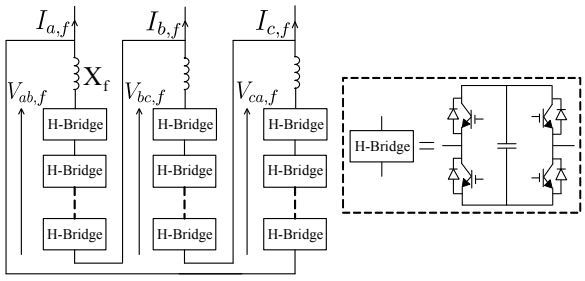

(b) Delta-connected CHB VSC topology

Fig. 9. The DSM simulation model.

pattern, while the d-component of the CHB VSC reference current ($i_{d,f}^{ref}$) has been determined by the DC-link voltage control given in [35].

Furthermore, as can be seen in Fig. 9a, The OWF has been represented by an aggregated model consisting of a *current-controlled AC-voltage source* $\boldsymbol{V_g}$ and a reactance $\mathrm{X_g}$ given that the proposed control system can be implemented irrespective of the type of WTs used. Then, the AC-voltage $\boldsymbol{V_g}$ is generated through the conventional power controller where d- and q-components of the offshore AC-grid currents are controlled to transfer the desired OWF incoming active and reactive power references. Note that $\boldsymbol{V_g}$ is synchronized with the controller reference frame by using the conventional voltage oriented control via PLL, provided that the system frequency is controlled by the CHB VSC. This way the offshore AC-grid current control becomes the same as the WTGS control systems used in the conventional VSC-based HVDC grid forming [36]. Therefore, using the proposed control system, no changes are needed to be applied in the conventional WT control systems.

Fig. 10 shows the performance of the proposed control system for both the DSM and the AVM during the case with the higher initial incoming active power considered in Subsection VI-A. But, the scheduled input changes have been simulated here for 4 s where the incoming active and reactive powers have increased at t = 0.5 s and t = 2.5 s, respectively. Finally, an appropriate performance of the proposed control system can also be concluded from the DSM simulation with the observations obtained by the AVM simulation, while the accuracy of the proposed AVM is verified. However, due to the implementation of the offshore AC-grid current controller in the OWF aggregated model for the DSM, the incoming active power change affects the dynamic response of the incoming reactive power and vice versa. This results in a slight difference between the dynamic responses of the DSM

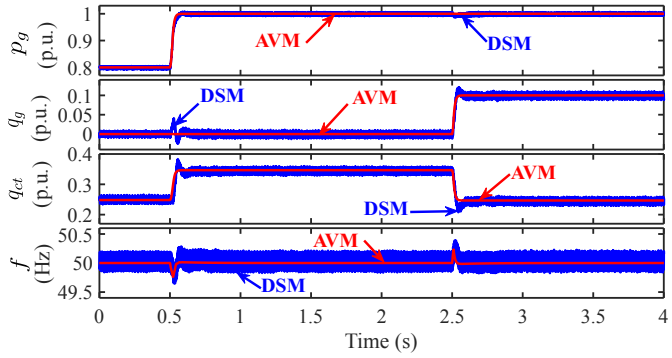

(a) Incoming active and reactive powers, controlled reactive power and frequency

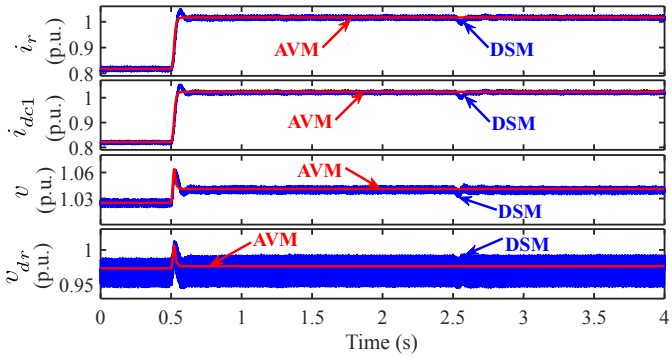

(b) Rectifier AC-current magnitude, rectifier DC-current, PCC voltage magnitude and rectifier DC-voltage

Fig. 10. Control system performance during active and reactive power changes for both the DSM and the AVM.

and the AVM during the corresponding transients. Note that, from the system studies of Fig. 3 and the simulations, it can be concluded that the proposed control system provides comparative advantages in terms of the DR station volume and the OWF installation cost with any other centralized control in which besides a VSC, a high voltage large capacitor bank is also needed to be placed at the DR station [28].

Fig. 11 shows rectifier, CHB VSC and offshore AC-grid phase currents ($\boldsymbol{i_r}$, $\boldsymbol{i_f}$ and $\boldsymbol{i_g}$), and PCC phase voltages ($\boldsymbol{v}$) for the DSM during the rated incoming active power when q_g equals 0.1 p.u. As observed, the DR harmonic currents do not exist in $\boldsymbol{i_g}$ because of the APF scheme (Fig. 2) implemented by the CHB VSC. But, $\boldsymbol{i_f}$ contains the corresponding harmonic components for the SHC. Therefore, the CHB VSC needs an increased power rating of less than 2 % for the harmonic current compensation at OWF rated power, although the required reactive power for the frequency control accounts for the largest part of the total CHB VSC rated power [27]. Finally, as can be seen in Fig. 11, $\boldsymbol{v}$ does not have low-order harmonics generated by the DR, thereby verifying the performance of the proposed overall control scheme.

VII. Conclusion

This paper has presented a direct frequency control for an OWF connected to the onshore through a DR-based HVDC link. A VSC has been placed at the DR station to guarantee the frequency control through satisfying reactive power balance at the DR station bus without a capacitor bank placed at the

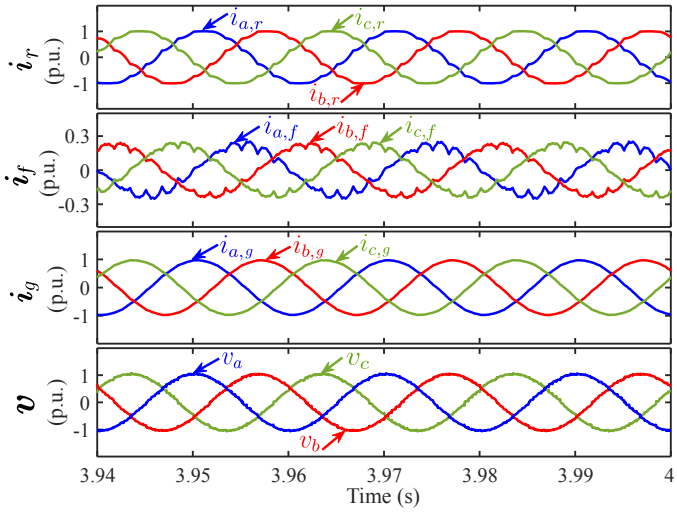

Fig. 11. Rectifier, CHB VSC and offshore AC-grid phase currents, and PCC phase voltages for the DSM during the rated incoming active power when the incoming reactive power is equal to 0.1 p.u.

DR station. Then, considering the OWF active and reactive powers as inputs, the control system has been derived from a simplified model representing the AC-side dynamics of the DR whose state variables are the polar components of the rectifier current vector (i.e. magnitude and angle of the current vector). In addition, given an APF scheme implemented by the VSC, passive AC-filters have also been removed from the DR station. Therefore, the required DR station volume and as a result, the OWF installation cost can be relatively reduced compared to other centralized controls in which besides a VSC, a high voltage large capacitor bank is also needed to be placed at the DR station. A new AVM of the DR system for such applications has also been derived to test the performance of the proposed frequency control principles, in which the the dynamics of a capacitor bank is not needed to produce the outputs. Moreover, the stability of the proposed control system has been proved by a small-signal analysis. Finally, the performance of the proposed control system has been demonstrated using the operation and control of a delta-connected CHB VSC in a DSM simulation of the system, while the accuracy of the proposed AVM has been verified. Both the AVM and the DSM simulations have verified a proper performance of the proposed control system.

Appendix A

The extra algebraic equations needed for the proposed AVM are as follows:

$$k_\mu = \frac{1}{2}\left(1+\cos\mu\right)\sqrt{1+\left(\mu\csc^2\mu-\cot\mu\right)^2} \tag{A.1}$$

$$r_\mu\, i_{dc1} = \frac{v}{2}\left(1-\cos\mu\right) \tag{A.2}$$

$$v_{dr} = v - r_\mu\, i_{dc1} = k_\mu\, v\, \cos\varphi \tag{A.3}$$

where $r_\mu = \dfrac{\pi}{6}\dfrac{\mathrm{x_t}}{n_b}$ is the commutation resistance and n_b is the number of six-pulse diode bridges.

TABLE I
SYSTEM AND CONTROL PARAMETERS

Description	Value
$S_{base,ac}$	100 MVA
$V_{base,ac}$	33 kV
$P_{base,dc}$	100 MW
$V_{base,dc}$	89.131 kV
n_b	2 six-pulse bridges
$\mathrm{T_r}$	$\mathrm{x_t}/n_b$ = 0.12 p.u. (33 kV/33 kV)
$\mathrm{x_g}$	0.1 p.u.
$\mathrm{x_f}$	0.15 p.u.
$\mathrm{r_{dc1}}$ = $\mathrm{r_{dc2}}$	0.00765 p.u.
$\mathrm{l_{dc1}}$ = $\mathrm{l_{dc2}}$	0.57367 p.u.
$\mathrm{c_c}$	2.66347 p.u.
v_{di}	0.9609 p.u.
f_0	50 Hz
k_p	2 p.u.
k_i	$10/\omega_0$ = 0.0318 p.u.
H-Bridges capacitor	8 mF
H-Bridges DC-link voltage	2.7 kV
Number of H-Bridges per phase	23
Switching frequency	2.5 kHz

APPENDIX B

Table I shows the system and control parameters used in the simulations.

REFERENCES

[1] O. Gomis-Bellmunt, J. Liang, J. Ekanayake, R. King, and N. Jenkins, "Topologies of multiterminal hvdc-vsc transmission for large offshore wind farms," *Electric Power Systems Research*, vol. 81, no. 2, pp. 271–281, 2011.

[2] P. Menke, R. Zurowski, T. Christ, S. Seman, G. Giering, T. Hammer, W. Zink, F. Hacker, D. Imamovic, E. Thisted *et al.*, "Breakthrough in dc grid access technology for large scale offshore wind farms," *EWEA Offshore*, 2015.

[3] O. Saborío-Romano, A. Bidadfar, Ö. Göksu, M. Altin, N. A. Cutululis, and P. E. Sørensen, "Connection of owpps to hvdc networks using vscs and diode rectifiers: an overview," in *15th International Workshop on Large-Scale Integration of Wind Power into Power Systems as well as on Transmission Networks for Offshore Wind Power Plants*, 2016.

[4] A. Siemens, "Energy management," *Presentation: Siemens presents new DC grid connection for offshore wind farms*, 2015.

[5] R. Blasco-Gimenez, S. Ano-Villalba, J. Rodríguez-D'Derlée, F. Morant, and S. Bernal-Perez, "Distributed voltage and frequency control of offshore wind farms connected with a diode-based hvdc link," *IEEE Transactions on Power Electronics*, vol. 25, no. 12, pp. 3095–3105, 2010.

[6] R. Blasco-Gimenez, N. Aparicio, S. Ano-Villalba, and S. Bernal-Perez, "Lcc-hvdc connection of offshore wind farms with reduced filter banks," *IEEE Transactions on Industrial Electronics*, vol. 60, no. 6, pp. 2372–2380, 2013.

[7] R. Vidal-Albalate, R. Pena, E. Belenguer, S. Añó-Villalba, R. Bernal-Perez, and R. Blasco-Gimenez, "Simultaneous connection of type-3 and type-4 off-shore wind farms to hvdc diode rectifier units," in *Proceedings of the 15th Wind Integration Workshop*, 2016, pp. 1–6.

[8] A. I. Andrade, R. Blasco-Gimenez, and G. R. Pena, "Distributed control strategy for a wind generation systems based on pmsg with uncontrolled rectifier hvdc connection," in *Industrial Technology (ICIT), 2015 IEEE International Conference on*. IEEE, 2015, pp. 982–986.

[9] A. A. Iván, P. G. Ruben, R. Blasco-Gimenez, and R. A. Javier, "Control strategy of a hvdc-diode rectifier connected type-4 off-shore wind farm," in *Future Energy Electronics Conference (IFEEC), 2015 IEEE 2nd International*. IEEE, 2015, pp. 1–6.

[10] L. Yu, R. Li, and L. Xu, "Distributed pll-based control of offshore wind turbines connected with diode-rectifier-based hvdc systems," *IEEE Transactions on Power Delivery*, vol. 33, no. 3, pp. 1328–1336, 2018.

[11] M. Á. Cardiel-Álvarez, S. Arnaltes, J. L. Rodriguez-Amenedo, and A. Nami, "Decentralized control of offshore wind farms connected to diode-based hvdc links," *IEEE Transactions on Energy Conversion*, vol. 33, no. 3, pp. 1233–1241, 2018.

[12] C. Prignitz, H.-G. Eckel, S. Achenbach, F. Augsburger, and A. Schön, "Fixref: a control strategy for offshore wind farms with different wind turbine types and diode rectifier hvdc transmission," in *Power Electronics for Distributed Generation Systems (PEDG), 2016 IEEE 7th International Symposium on*. IEEE, 2016, pp. 1–7.

[13] C. Prignitz, H. Eckel, and S. Achenbach, "Fixref: A current control strategy for offshore wind turbines connected to different types of hvdc transmission," in *Proceedings of the 15th Wind Integration Workshop, Vienna, Austria*, 2016, pp. 15–17.

[14] S. Seman, R. Zurowski, and C. Taratoris, "Interconnection of advanced type 4 wtgs with diode rectifier based hvdc solution and weak ac grids," *14th Wind Integr. Work.*, pp. 2–8, 2015.

[15] D. Xiang, L. Ran, J. R. Bumby, P. J. Tavner, and S. Yang, "Coordinated control of an hvdc link and doubly fed induction generators in a large offshore wind farm," *IEEE transactions on power delivery*, vol. 21, no. 1, pp. 463–471, 2006.

[16] R. Li, S. Bozhko, G. Asher, and L. Yao, "Grid frequency control design for offshore wind farms with naturally commutated hvdc link connection," in *Power Electronics and Applications, 2007 European Conference on*. IEEE, 2007, pp. 1–10.

[17] R. Li, S. Bozhko, and G. Asher, "Frequency control design for offshore wind farm grid with lcc-hvdc link connection," *IEEE Transactions on Power Electronics*, vol. 23, no. 3, pp. 1085–1092, 2008.

[18] S. Foster, L. Xu, and B. Fox, "Control of an lcc hvdc system for connecting large offshore wind farms with special consideration of grid fault," in *Power and Energy Society General Meeting-Conversion and Delivery of Electrical Energy in the 21st Century, 2008 IEEE*. IEEE, 2008, pp. 1–8.

[19] S. V. Bozhko, R. Blasco-Gimenez, R. Li, J. C. Clare, and G. M. Asher, "Control of offshore dfig-based wind farm grid with line-commutated hvdc connection," *IEEE Transactions on Energy Conversion*, vol. 22, no. 1, pp. 71–78, 2007.

[20] S. Bozhko, G. Asher, R. Li, J. Clare, and L. Yao, "Large offshore dfig-based wind farm with line-commutated hvdc connection to the main grid: Engineering studies," *IEEE transactions on energy conversion*, vol. 23, no. 1, pp. 119–127, 2008.

[21] H. Zhou, G. Yang, J. Wang, and H. Geng, "Control of a hybrid high-voltage dc connection for large doubly fed induction generator-based wind farms," *IET renewable power generation*, vol. 5, no. 1, pp. 36–47, 2011.

[22] H. Zhou, G. Yang, and J. Wang, "Modeling, analysis, and control for the rectifier of hybrid hvdc systems for dfig-based wind farms," *IEEE Transactions on Energy Conversion*, vol. 26, no. 1, pp. 340–353, 2011.

[23] T. H. Nguyen, D.-C. Lee, and C.-K. Kim, "A series-connected topology of a diode rectifier and a voltage-source converter for an hvdc transmission system," *IEEE Transactions on Power Electronics*, vol. 29, no. 4, pp. 1579–1584, 2014.

[24] T. H. Nguyen, Q. A. Le, and D.-C. Lee, "A novel hvdc-link based on hybrid voltage-source converters," in *Energy Conversion Congress and Exposition (ECCE), 2015 IEEE*. IEEE, 2015, pp. 3338–3343.

[25] M. von Hofen, D. Karwatzki, L. Baruschka, and A. Mertens, "Hybrid offshore hvdc converter with diode rectifier and modular multilevel converter," in *Power Electronics for Distributed Generation Systems (PEDG), 2016 IEEE 7th International Symposium on*. IEEE, 2016, pp. 1–7.

[26] M. Hoffmann, C. Rathke, A. Menze, N. G. Hemdan, and M. Kurrat, "Parallel operation of hvdc dru and vsc converters for offshore wind farm connection: Technical and economic feasibility," 2019.

[27] Y. Chang and X. Cai, "Hybrid topology of a diode-rectifier-based hvdc system for offshore wind farms," *IEEE Journal of Emerging and Selected Topics in Power Electronics*, 2018.

[28] M. A. Cardiel-Alvarez, J. L. Rodriguez-Amenedo, S. Arnaltes, and M. E. Montilla-DJesus, "Modeling and control of lcc rectifiers for offshore wind farms connected by hvdc links," *IEEE Transactions on Energy Conversion*, vol. 32, no. 4, pp. 1284–1296, 2017.

[29] A. Nami, J. Rodríguez Amenedo, S. Arnaltes Gómez, and M. Cardiel Álvarez, "Active power filtering embedded in the frequency control of an offshore wind farm connected to a diode-rectifier-based hvdc link," *Energies*, vol. 11, no. 10, p. 2718, 2018.

[30] E. W. Kimbark, *Direct current transmission*. John Wiley & Sons, 1971, vol. 1.

[31] X.-F. Wang, Y. Song, and M. Irving, *Modern power systems analysis*. Springer Science & Business Media, 2010.

[32] A. Yazdani, "Control of an islanded distributed energy resource unit with load compensating feed-forward," in *2008 IEEE Power and Energy Society General Meeting-Conversion and Delivery of Electrical Energy in the 21st Century*. IEEE, 2008, pp. 1–7.

[33] M. Szechtman, T. Wess, and C. Thio, "A benchmark model for hvdc system studies," in *International conference on AC and DC power transmission*. IET, 1991, pp. 374–378.
[34] N. Marks, T. Summers, and R. Betz, "Challenges for capacitor voltage balancing in a cascaded h-bridge statcom utilising finite control set model predictive control," in *2013 Australasian Universities Power Engineering Conference (AUPEC)*. IEEE, 2013, pp. 1–6.
[35] E. Behrouzian, *On control of cascaded H-bridge converters for STATCOM applications*. Chalmers University of Technology, 2017.
[36] S. Muyeen, R. Takahashi, and J. Tamura, "Operation and control of hvdc-connected offshore wind farm," *IEEE Transactions on Sustainable Energy*, vol. 1, no. 1, pp. 30–37, 2010.